Surface and Coatings Technology 206 (2011) 149-154

# Amorphous Boron containing Silicon Carbo-Nitrides created by ion sputtering

V.M. Vishnyakov[*)], A.P. Ehiasarian[1)], V.V. Vishnyakov, P. Hovsepian[1)], J. S. Colligon

School of Computing and Enginering, The University of Huddersfield, Queensgate, Huddersfield H1 3DH

*Former address: Manchester Metropolitan University, Manchester, M1 5GD, UK*

[1)] *Nanotechnology Centre for PVD Research, Sheffield Hallam University, Sheffield, S1 1WB, UK*

## Abstract

Silicon carbo-nitride films with Boron were deposited onto Silicon, glass and SS304 Stainless Steel substrates using the ion beam assisted deposition (IBAD) method. The coating composition, rate of ion-assistance and substrate temperature were varied. Films were examined by X-Ray Diffraction, Scanning Electron microscopy, Energy Dispersive X-Ray analysis, Cathodoluminescence, Atomic Force Microscopy and Nano-indentation. The composition and chemical bonding variation was found to be dependent on deposition conditions. All coatings were amorphous, fully dense and showed high hardness up to 33 GPa. It is suggested that the low friction coefficient of about 0.3, measured against $Al_2O_3$ using the pin-on-disk method, may be the result of the presence of C nanoclusters which are formed under the low energy deposition conditions. Films deposited on Stainless Steel had an onset of rapid thermal oxidation at $1150^0$ C in air as determined by thermogravimetric analysis. The films have a Tauc bandgap between 2.2 and 2.8 eV and were also exceptionally high electrical resistive which may indicate the presence of localized states.

Key words: boron, silicon carbo-nitride, ion beam sputtering, low friction, hard coatings, oxidation resistant coating, band-gap

[*)] *Corresponding author: email: v.vishnyakov@mmu.ac.uk.*

## Introduction

Quaternary Carbo-Nitrides have recently emerged as novel multi-functional tough materials [1, 2]. The materials have potential to be used as protective coatings [3, 4] with potent electrical and optical properties [5, 6] and have even been proposed for use as low-k materials [7]. The general formula of such materials can be represented in the form *Si**Me**CN,* where ***Me*** can be Ti, Zr or B. In these materials Si and ***Me*** both exist in carbide and nitride forms [6, 8]. Light atoms forming short and covalent bonds are responsible for the very high formation enthalpies, exceeding 200 kJ/mol. High binding energies make these materials exceptionally stable and tough. The materials can be in principle modelled and partially understood on the basis of Silicon Carbonitrides which have been thoroughly studied and this approach of modeling is especially valid in the case when the ***Me*** concentration is relatively low. Following this train of thought, it has been shown that, for some material compositions, it is possible to represent an atomic arrangement where Si is submerged into the tetragonal pyramid formed by either one of the other three atoms [6, 9]. The validity of this concept for materials prepared by various methods still needs to be substantiated by more experimental data.

Various carbonitrides were synthesised by a polymer-to-ceramic transformation route (see for example [2, 10-12]). This approach offered bulk material synthesis but rather limited base composition freedom and high impurity, such as Oxygen and Hydrogen, concentrations. In the case of SiBCN it has been shown that the synthesised material is oxidation resistant in air up to $1700^0$ C and compositionally stable up to $2000^0$ C [2], which is much higher than the SiCN oxidation threshold at around $1350^0$ C [13]. At the same time material usage at temperatures higher than the pyrolysis temperature leads to material densification and creation of multiple cracks. Lately the Physical Vapour Deposition (PVD) approach has been successfully used [3]. The materials show high hardness, up to 44 GPa, and, in the case of SiBCN, have exceptionally high temperature stability. Oxidation protection by formation of surface $SiO_2$ is most effective at silicon concentration around 30 at%. Moreover, the material remains amorphous even at temperatures around $1300^0$C,

but in certain compositions starts to crystallize at $1400^0$C [10]. Some compositions show stability even at $1600^0$C [14]. This is in line with the similar ternary system SiCN where, by varying C concentration, it was discovered that at carbon content more than 2 at.% the system will not crystallise at temperatures of $1250^0$ C [15]. What makes the material even more interesting is its low thermal expansion coefficient coupled with low inherited stress and potentially good adhesion to the substrate [16]. This makes the material very unlikely to have high stress at high temperatures and, consequently, to be very mechanically stable on the substrate. The material with low carbon content has high resistance and shows a potential to be used in microelectronics, where system-on-chip applications require high resistivity substrates [17].

Most of the work on carbo-nitrides with B has been done on bulk material. There are a very limited number of papers on thin film boron-carbo-nitrides and the field of creation and properties of those materials is virtually unexplored.

Ion beam assisted deposition (IBAD) offers an easy method for varying film composition and has the additional capability of introduction of additional energy and atomic species into the growing film. This potential was used for the first time in the present communication to create Silicon Metal-Carbo-Nitrides on various substrates.

**Experimental**

The samples reported in this paper were deposited on Si, glass slides and SS304 stainless steel substrates in the dual ion beam chamber. The schematic drawing of the deposition system is presented in Fig.1.

The system comprises a top Ion Gun, which produces an ion beam of approximately 100 mm in diameter, an Ion-assist Source, sputter target and heated substrate holder. The carbon forms the base of the target plate on which multiple pieces of silicon and boron are mounted. The growing film composition is defined by the relative areas and sputter yields of elemental targets under the ion beam. Argon is supplied to the chamber through the top ion gun. Nitrogen is supplied through the Ion Assisting Source. These cases are referred to as “ion-assisted”. In some cases a discharge was run in the source without applying an acceleration voltage to produce

nitrogen ions at low energy of a few eV. These cases are referred to as “plasma-assisted”.

The vacuum in the chamber was measured by a Pfeiffer Active Pirani/ Cold Cathode gauge. The readings reported in the paper were not corrected for the gauge sensitivity factors. The base pressure in the chamber was $2.8 \times 10^{-4}$ Pa. During deposition the argon partial pressure was $2.8 \times 10^{-2}$ Pa and nitrogen partial pressure was $2 \times 10^{-2}$ Pa.

The substrate holder surface temperature was calibrated with a platinum resistance probe. The substrates were clamped against the flat holder surface.

Microscopy was carried out in a Zeiss Supra VP40 Field Emission Gun Scanning Electron Microscope (FEG SEM). Film thickness was measured on cross-sectioned samples. Energy dispersive analysis was performed using an EDAX Sapphire Si(Li) detector and quantified by the standardless ZAF algorithm. The detector sensitivity below 1 keV X-Ray energy was calibrated on well-characterised samples and standards, however it is still possible that there might be a significant systematic error in boron quantification and further work is currently being carried out to resolve this issue.

The Cathodoluminescence (CL) was measured on the above SEM at 20keV and 4 nA electron beam with a Gatan MonoCL3+ assembly. It was assumed that the CL optical path transmission function did not have any singularities in the 350 to 700 nm region, apart from the applied correction for Hamamatsu R374 Photon Multiplier Tube.

The Raman spectra were measured using a Renishaw InVia Raman microscope with Ar laser excitation at 514.3 nm. The data were acquired from 2 µm diameter spots with neutral filters limiting laser power to 10%, e.g. around 0.2 mW/µm$^2$ or, $2 \times 10^8$ W/m$^2$. This level of power was carefully chosen after a set of experiments in which the power was slowly stepped up in a series of spectra acquisitions. After high power laser irradiation it was possible to see modifications of the initial spectra. It is presumed that the very low powers, below 0.2 mW/µm$^2$ in the series, do not modify samples, and a safe laser power is chosen for use to avoid evident Raman spectra alterations.

Thermogravimetric tests were performed on a Setaram 1700 SetSys Evolution Instrument. A stainless steel substrate of total area approximately 20 $cm^2$ (10 $cm^2$ per side) was coated on both sides in four successive depositions in order to provide maximum surface coating in difficult-to-coat areas.

Atomic force microscopy (AFM) and nanoindentation data were acquired using a CSM nanoindenter.

In order to assess film tribological properties, a number of films were deposited onto SS304 Stainless Steel blanks which had been polished using a 1 μm diamond paste. These were subjected to pin-on-disk tests using Alumina balls with diameter 6 mm as counterparts at normal load 5 N. The tests were conducted at room temperature and at a humidity, which was measured to be in the region of 50 % but was not controlled.

**Results and Discussion**

All produced coatings have a dense glassy structure as can be seen in Fig.2. The Atomic Force Microscopy results show very flat surfaces with maximum roughness, as defined from peak to trough, at around 1 nm and RMS value at around 0.5 nm. According to our data this is almost indistinguishable from the roughness of the Silicon substrate itself. The glassy structure appearance in the SEM is supported by the absence of diffraction peaks in XRD, see Fig.3, which indicates absence of sizeable crystallites. At the same time, the almost atomically smooth surface adds to the argument that the material is very homogeneous, as the presence of density inhomogeneous zones and even small crystallites would lead to surface roughening. On this evidence it can be concluded that the material is amorphous and this is in agreement with published work.

As mentioned before, samples were prepared on a wide variety of substrates and using a range of deposition conditions. The film adhesion to all substrates was not specifically measured but appears to be good and as-deposited films have not shown any traces of delamination and are very stable. Table 1 summarises the main

deposition parameters and film properties of the samples prepared on Silicon substrates. There is a possibility to vary many parameters but the preference in the set was given to vary substrate temperature, plasma and ion assistance. In general terms the elemental target areas were kept at values providing Boron concentration at around 10 at % and Silicon at below 40%. The target elemental content was not changed for the first 6 samples presented in Table 1 and all compositional variations result from varying deposition parameters. Nitrogen content in the film is significantly affected by the deposition conditions and is increased in samples N5 and N6 as a result of partially-ionised $N_2$ and, especially, $N^+$ ion bombardment in the IBAD process. In general terms this is in good agreement with predictions of effective Nitrogen incorporation during low energy ion assistance [18]. Ion assistance in this case significantly increases Nitrogen content in the material, however, this is accompanied by a reduction in Silicon content and may be linked to the reduction in hardness to a value just above 20 GPa. However, for sample N7, when the Silicon content is restored to higher values, by adjustment of target areas, the hardness is also increased to above 30 GPa, which follows the hardness dependence on Si content for SiCN [19]. It is also worth noticing that, for sample N7, the H/E value (Hardness over Young's Modulus), regarded by many as a parameter of material toughness, is the highest in the whole set of coatings. In general all samples with Silicon content equal to, or above, 30 at% showed hardness in excess of 30 GPa. Contrary to earlier published work [20], there is no clear trend linking higher deposition temperature to higher film hardness.

The most industrially-important results are related to the case of mild plasma assistance, as similar conditions would be expected for industrial scale DC magnetron deposition. One can easily see that the film composition in this case is almost temperature independent but slightly higher hardness can be achieved at elevated substrate temperature.

The pin-on-disk trace of the lowest friction film is shown in Fig.4. The coating was deposited at a substrate temperature of 450 $^0$C with plasma- assistance. One can see that the friction coefficient is, in this case, quite low at around 0.32. Samples produced at different deposition conditions have shown friction coefficients near to 0.5. The same friction test setting conditions have typically produced friction coefficients: 0.65 for TiAlN, 0.5 for CrN and 0.2 for DLC. As will be shown later in the

paper, for these deposition conditions we can expect a significant presence of C-C bonds. This possibly allows Carbon lubrication of the friction contact and supports the low friction coefficient observed earlier for the ceramics. [21]

The coatings also show good stability at high temperatures. The SS coupon coated with approximately 3 μm film, in conditions similar to sample 4 in Table 1, starts to oxidise rapidly only at temperatures above 1150 $^0$C as indicated in Fig.5. Taking into account that the SS substrate will already start to oxidise at 850$^o$C, the preliminary data indicate significant coating/substrate stability at elevated temperature against oxidation.

When deposited onto slide glass, the films were light brown, as seen in transmitted light, which indicated film light absorption in the green/blue region of the visible light spectrum. Absorption spectra show light interference features but, as can be seen in Fig.6 the overall tendency might suggest that the optical bandgap depends on deposition conditions and film composition. From the optical spectra it can be cautiously assumed that the observed high absorption is due to bandgap transitions and, in this case, the bandgap value is located in the region between 2.2 and 2.8 eV. The values are in rather good agreement with the data published by Vijayakumar *et al.* [5]. The results also demonstrate the existence of a tunable bandgap for the material and this might follow the general trends observed for the SiCN system [22]. It is interesting to note that, for the SiCN system produced by Plasma Enhanced Chemical Vapour Deposition, samples show a bandgap at around 3.3 eV whereas the hardness was only about 2 GPa [23] . This suggests that the bandgap is mostly dictated by the SiCN matrix, but the huge variation in matrix density, which changes the hardness 10 times, hardly affects the general bandgap structure.

The CL spectra presented in Fig.7 show that the CL starts at around 3.2 eV and can reasonably be deconvoluted into a number of emission lines. Taking into account that the material is amorphous this most probably indicates that there are localised states responsible for the high energy part of the CL spectra and these states form a tail at the bottom of the conduction zone. The nature of these centres is not clear. It was shown, for very intensive photoluminescence of $Si_{33.7}C_{22.9}N_{22.8}O_{20.6}$ [24], that the luminescence at 3.4 eV, which is not observed in our study, is related to O vacancies associated with a Si-O sub-network, while luminescence at 2.65 eV was ascribed to

the C-C $sp^2$ bonding. Samples in the current study have much smaller Oxygen content (see later in this paper) and the luminescence spectra presented in the current paper is related to the IBAD sample which, as will also be shown later in the paper, does not have a C-C $sp^2$ Raman signal. This indicates that the nature of transitions responsible for the CL at the moment is not clear.

Raman spectra are presented in Fig.8. The spectra of the ion beam sputtered sample without ion- or plasma-assistance shows only possible C-C bonds in the region of 1500 $cm^{-1}$ (the D and G bands not being obviously resolved). The signal at around 2800 $cm^{-1}$ corresponds to 2D and G+D modes and was reported for fully dense Si-C-N ceramic synthesized by pyrolysis for a comparatively similar composition but containing Boron [25]. Laser annealing of the analysis spot leads to a significant change in structure, which leads to a strengthening of all carbon signals. All this shows that samples without ion assistance have a significant number of C-C bonds and yet demonstrate hardness in excess of 30 GPa, while the highest hardness reported by Janakiraman [25] for the bulk material is just above 11 GPa.

The presence of C-C bonds and potentially Carbon nano-clusters is unexpected but there is evidence that even SiCN, synthesized by different methods, tends to have a significant number of C-C bonds. In the experiment where SiCN was created by Nitrogen implantation into SiC [26] the XPS data, after a 1000 eV Ar etch, show the presence of graphitic Carbon. This could have been attributed to accumulation of Carbon on the surface due to preferential sputtering, but the authors also have done Electron Energy Loss Spectroscopy (EELS) experiments and demonstrated clustered $sp^2$ bonded Carbon, which indicates preferential formation of Si-N at the expense of Si-C bonds.

The absence of B-C and B-N related features in the spectra might suggest high kinetic barriers to the above reactions. It may also suggest the presence of weakly bonded Boron in the lattice and this raises a question about the state of Boron in the deposited films. This might contradict, at first glance, some X-Ray Photoelecton Spectroscopy (XPS) results, see for example the work of Vlcek et al [3], when Boron has been shown to be bound into the atomic lattice. However it is quite common practice during XPS experiments to clean the surface by bombarding it with the ion beam and this leads to ion-induced atomic mixing and bond modification. It is quite

possible that Boron bonding into the lattice needs activation and can be achieved only at high temperatures or intensive ion bombardment. This is supported by the data on pyrolysed SiBCN which showed that Boron was firmly built into an amorphous network [27]. One might conclude that “low energy deposition conditions”, e.g. low deposition temperature and absence of ion bombardment, leads to formation of three interlocked atomic subsystems comprising a SiN network with clustered nano Carbon and weakly bonded Boron.

The origin of the Raman signal at around 700 $cm^{-1}$ is difficult to explain. Infrared spectroscopy in the Si-C-N ceramic mentioned above [25] shows peaks in this energy region and they are produced by Si-N and Si-C bonds, but they have not been reported to be Raman active. In support of the latest view, Fainer et al [23] have reported a featureless Raman spectra for SiCN. In principle it is still possible that, for particular deposition conditions of sample N1, that the resulting material structure is such that Si-N and Si-C bonds show in the Raman Spectra of as-deposited material but these disappear after laser annealing when material is restructured.

Ion assistance changes the Raman spectra quite significantly. The peak at 1090 $cm^{-1}$ probably can be ascribed either to B-N or B-C bonding and the peak positioning is very characteristic for Boron-containing compounds [28]. Peaks at around 560 $cm^{-1}$ can be related to Si-N bonding, which will also be responsible for the shoulder at around 900 $cm^{-1}$ [29]. It is evident that the ion assistance promotes significant restructuring of chemical bonding. One can also expect that development in the Raman spectra can be seen as evidence of more ordered chemical bonding. Potentially this could have manifested itself in reduction of the absorption tails in the optical band-gap, but this is not observed. Another peculiarity is that a Raman signal in the region of 2200 $cm^{-1}$, which is ascribed to C-N [30], is not observed. All this shows complexity of bonding and atomic arrangements in the quaternary compounds [31] and these need to be investigated further.

All samples deposited in this study have shown exceptionally high electrical resistance. The very low electrical conductivity of deposited material caused micro-arcing in the vacuum chamber. The high resistance of these samples is not reported by other authors for films with similar stoichiometry [6, 12, 32-34]. In some cases [33,

34] the ceramic did not contain Boron and any conductivity was thought to be provided by Nitrogen in SiC. Another possibility for the difference in data is the role of Oxygen. In many studies involving pyrolysis, or even magnetron deposition, the Oxygen content was above 3 at%, while, in our study, it was below 1.5 at%. Taking into account that we have not discriminated for the near-surface and the bulk Oxygen and standard quantification correction procedures are not very accurate in the cases of surface layers, it is possible that our bulk Oxygen content was below 1 at%. Another possible method to overcome low conductivity was shown by Houska et al [16], where carbon content in the film was raised to 40 at% and Silicon was maintained at 10 at%.

In our case carbon and oxygen content are low while silicon content is relatively high. This might widen the band-gap but still leave the localised states tail below the conductance zone. The result is in agreement with earlier published work [35], where the conductivity of $SiBN_3C$ ceramic at temperatures below $395^0$ C was attributed to three-dimensional variable range hopping of carriers between localised states, which is a typical mechanism for amorphous semiconductors at low temperatures.

It is a well known and used fact that Hydrogen, as passivation agent, can be used to improve the electrical conductivity in defect-rich semiconductors (see for example [36, 37]) and should increase the band-gap in SiBCN ceramics according to electron structure modelling [38]. In the polymer-derived ceramics high hydrogen content is inherited from the ingredients while, during PVD processes, hydrogen comes from the water component of residual gases in the deposition chamber. The latest process is also accompanied by accumulation of Oxygen in the film. The fact that the Oxygen content was possibly below 1 at% in our films can also indicate that the Hydrogen content was relatively low. In order to check for any possible influence of Hydrogen on conductivity, a few depositions were conducted when Hydrogen was introduced into the deposition chamber at pressures up to $6.5 \times 10^{-2}$ Pa. The amount of Hydrogen in the film is not known but the insulating properties of the film were not changed.

## Conclusions

Boron-containing Silicon Carbo-Nitride thin films deposited by ion beam sputtering have an amorphous structure with exceptionally flat surfaces with roughness almost indistinguishable from the Si substrate. High hardness of up to 33 GPa and high H/E values of up to 0.14 can be achieved by varying deposition parameters and coating composition. On the basis of Raman data, it was shown that “low energy deposition conditions”, e.g. low deposition temperature, as in the present study, and absence of intensive ion bombardment, leads to formation of three interlocked atomic subsystems comprising a SiN network with clustered Carbon and weakly bonded Boron. The presence of nano-Carbon leads to solid lubrication of the tribological contact and a low friction coefficient in the region of 0.3. Nitrogen content in the film can be significantly increased by Nitrogen ion assistance. The presence of atomic Nitrogen from the plasma and a high substrate temperature allows coatings with the highest hardness (33 GPa) to be produced. The coatings, when deposited on SS304 Stainless Steel substrates showed an onset of rapid thermal oxidation at $1150^0$ C. The Tauc bandgap as found to have values between 2.2 and 2.8 eV. The low electrical conductivity, coupled with Cathodoluminescence data, can be explained on the basis of the presence of localized states. By using the IBAD method a range of compositions and bond arrangements could be obtained and, in principle, coating properties can be tailored to application requirements by choosing appropriate deposition conditions.

**Figure and Table Caption**

Table 1. Deposition parameters, atomic compositions and mechanical properties.

Table 2. Deposition parameters, atomic compositions and film bandgap values.

Fig. 1. Diagram of ion-beam assisted deposition system.

Fig. 2. a) - SEM image of sample N4 (see Table1) film on glass. The sample is tilted $45^0$ towards the secondary electron detector. b) – AFM on the sample N3 on silicon substrate, maximum height (black-to-white) amplitude is 1.1 nm, RMS value is equal to 0.5 nm.

Fig. 3. Typical X-Ray Diffraction spectrum of the films measured in Bragg-Brentano configuration

Fig. 4. Pin-on-disk coating friction test against alumina ball at normal load 5 N.

Fig. 5. Thermogravimetric test of coating on Stainless Steel.

Fig. 6. Optical absorption ($\alpha$) of in semi-logarithmic coordinates and linear approximations of absorption edge. Sample numbers correspond to Table 2.

Fig. 7. Cathodoluminesence spectra of sample N3 in Table 2. The spectra were obtained at
93 K, 20 nA electron beam at 10 keV.

Fig. 8. Raman spectra of various coatings: as deposited sample N1, Table 1; laser annealed sample at energy density approximately $2.5x10^9$ W/m$^2$ in air for 20 sec; IBAD sample N5, Table1.

| Sample Number | Substrate temperature $^0$C | Additional treatment | Si, at% | B, at% | C, at% | N, at% | Hardness, H, GPa | Young's Modulus, E, GPa | H/E |
|---|---|---|---|---|---|---|---|---|---|
| N1 | RT | No | 37 | 10 | 27 | 23 | 31.2 | 264 | 0.12 |
| N2 | 450 | No | 34 | 11 | 25 | 29 | 26 | 205 | 0.13 |
| N3 | RT | Plasma | 34 | 9 | 26 | 29 | 30.9 | 287 | 0.11 |
| N4 | 450 | Plasma | 34 | 9 | 25 | 29 | 33.6 | 250 | 0.13 |
| N5 | RT | IBAD | 26 | 7 | 10 | 54 | 21.1 | 179 | 0.12 |
| N6 | 450 | IBAD | 23 | 11 | 23 | 43 | 22 | 183 | 0.12 |
| N7 | 450 | IBAD | 30 | 9 | 17 | 40 | 32 | 233 | 0.14 |

**Table 1.**

| Sample Number | Substrate temperature, $^0$C | Additional treatment | Si, at% | B, at% | C, at% | N, at% | Optical Bandgap, eV |
|---|---|---|---|---|---|---|---|
| N1 | 450 | IBAD | 23 | 11 | 23 | 43 | 2.5 |
| N2 | 450 | IBAD | 30 | 9 | 17 | 40 | 2.2 |
| N3 | 450 | Plasma | 34 | 9 | 25 | 29 | 2.8 |

**Table 2.**

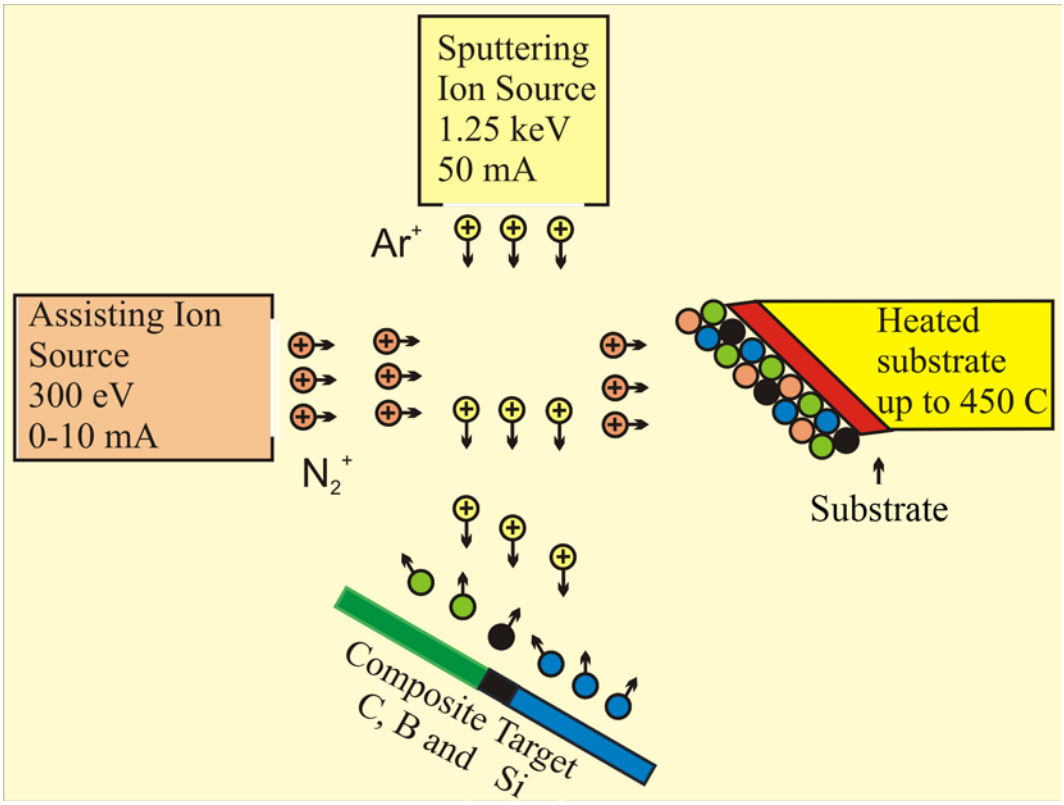
Sputtering
Ion Source
1.25 keV
50 mA
Ar+
Assisting Ion
Source
300 eV
0-10 mA
N2+
Heated
substrate
up to 450 C
Substrate
Composite Target
C, B and Si

**Fig. 1**

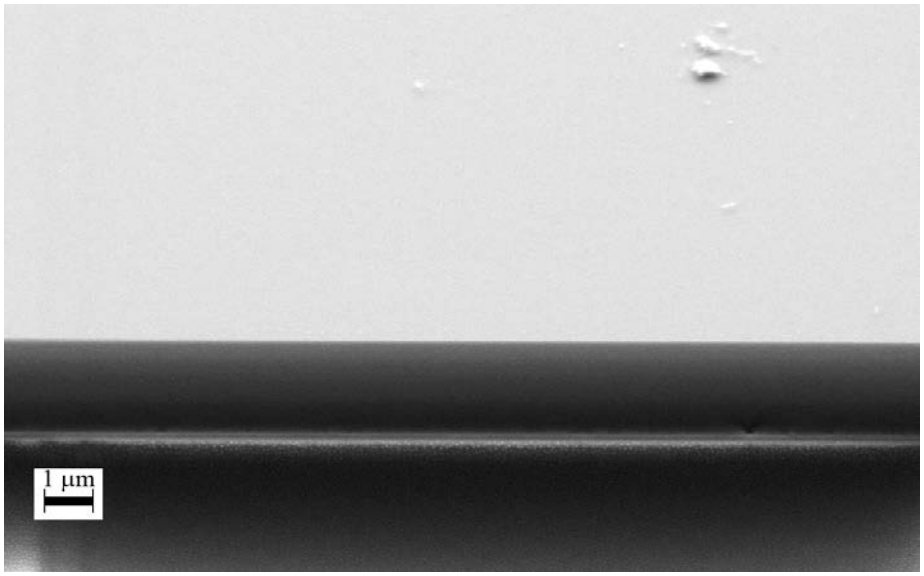


**Fig. 2a**

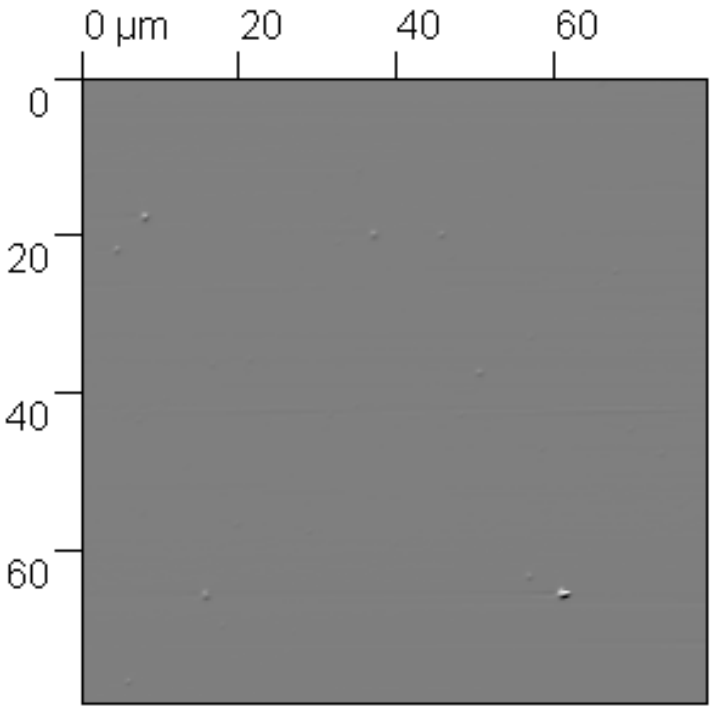


**Fig. 2b**

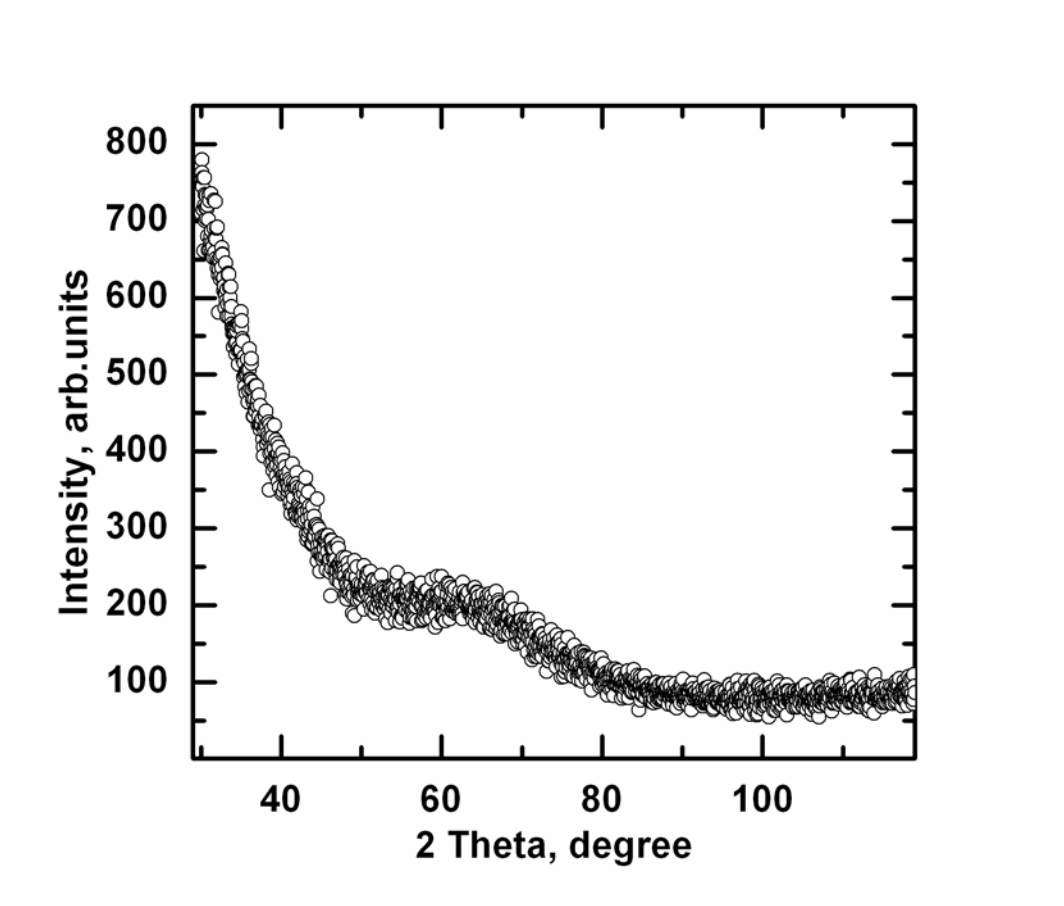
Intensity, arb.units
800
700
600
500
400
300
200
100
40
60
80
100
2 Theta, degree

**Fig. 3**

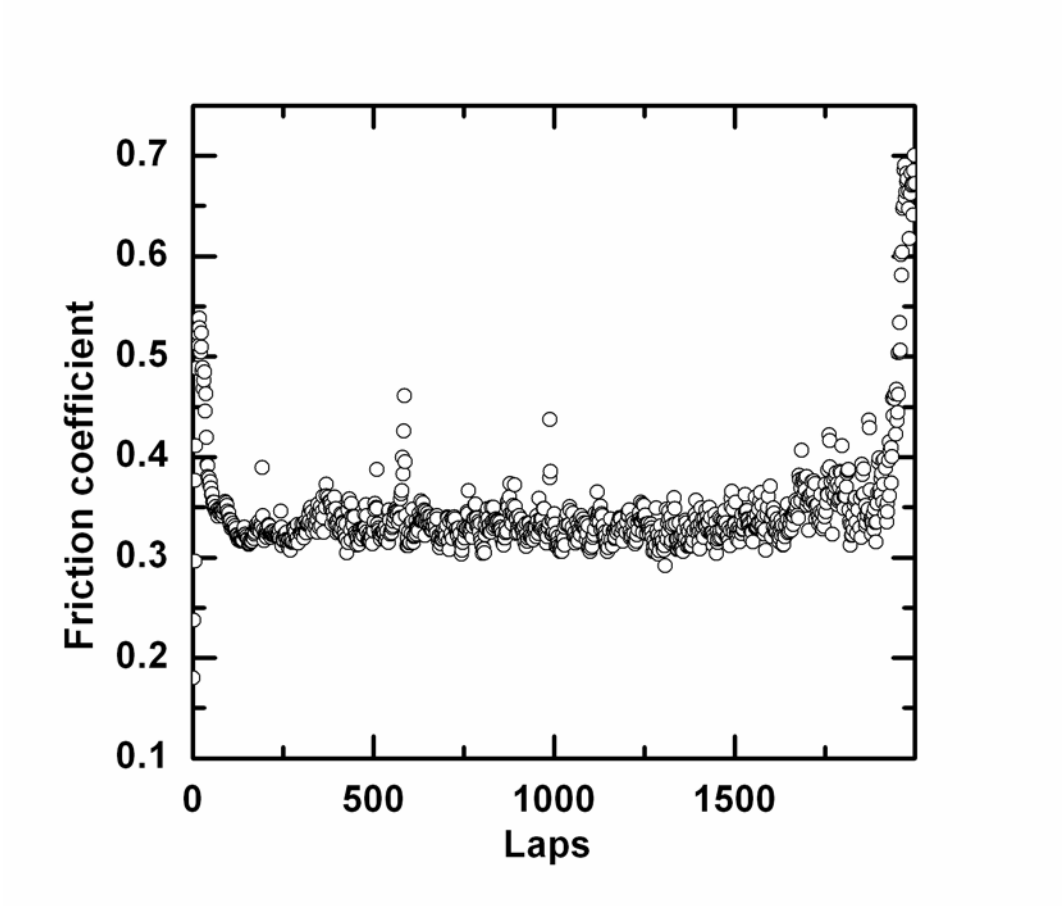


**Fig. 4.**

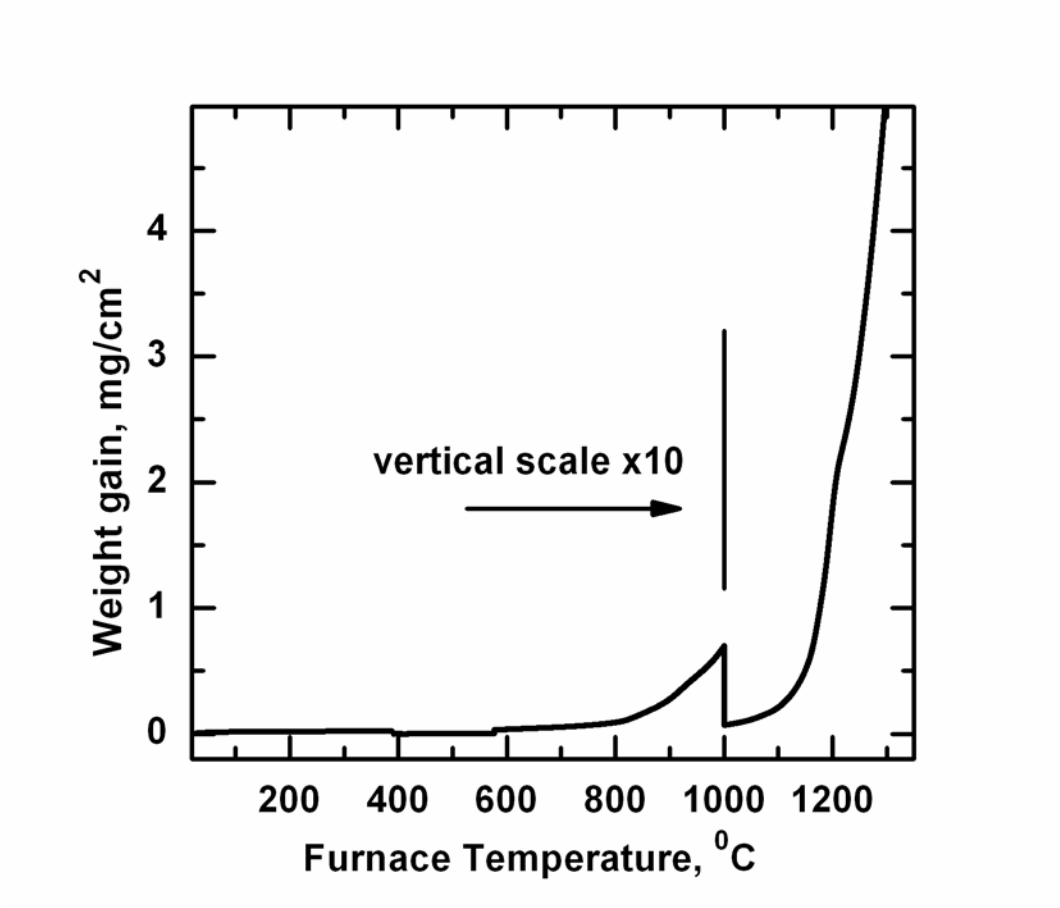
Weight gain, mg/cm$^2$
0
1
2
3
4
vertical scale x10
200
400
600
800
1000
1200
Furnace Temperature, $^0$C

**Fig. 5.**

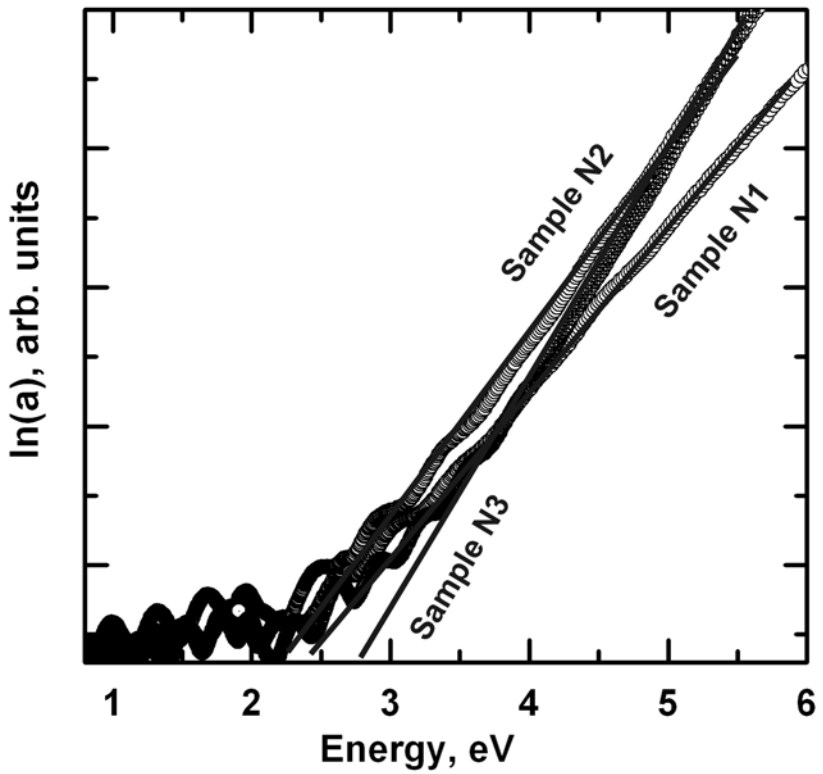


**Fig 6**

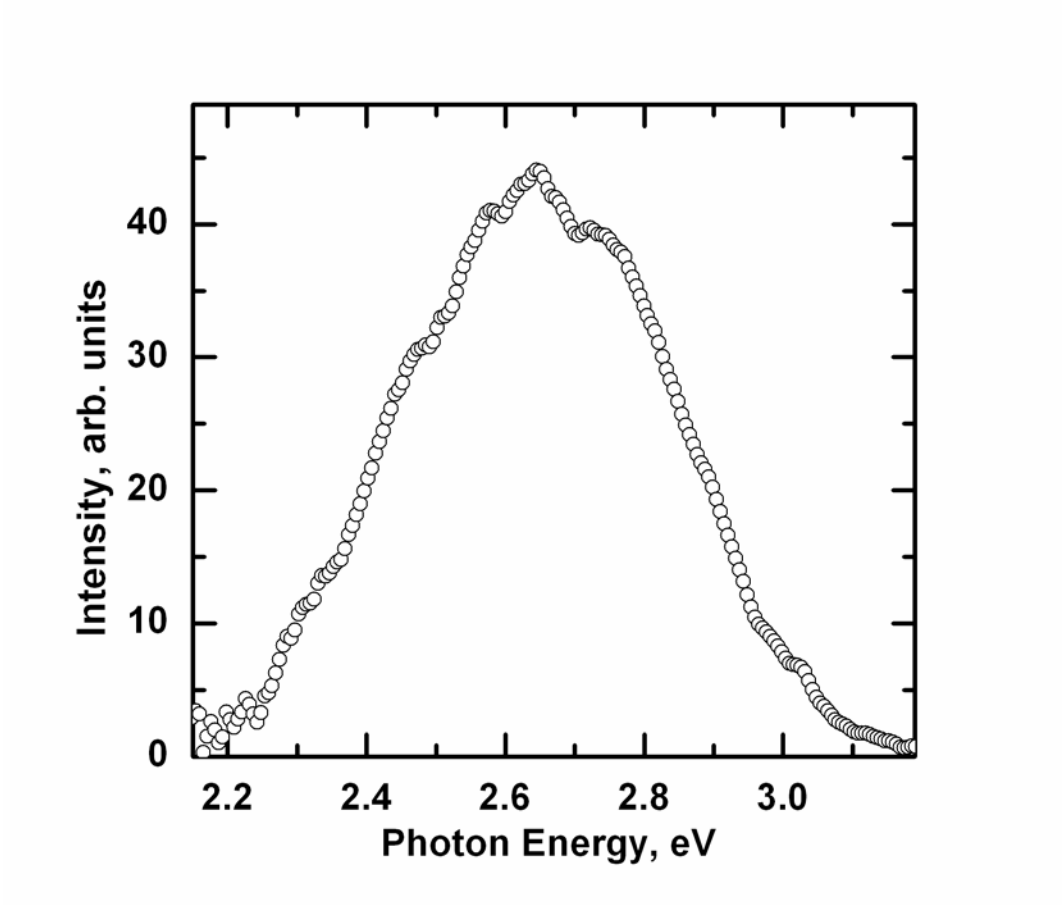
Intensity, arb. units
0
10
20
30
40
2.2
2.4
2.6
2.8
3.0
Photon Energy, eV

**Fig. 7.**

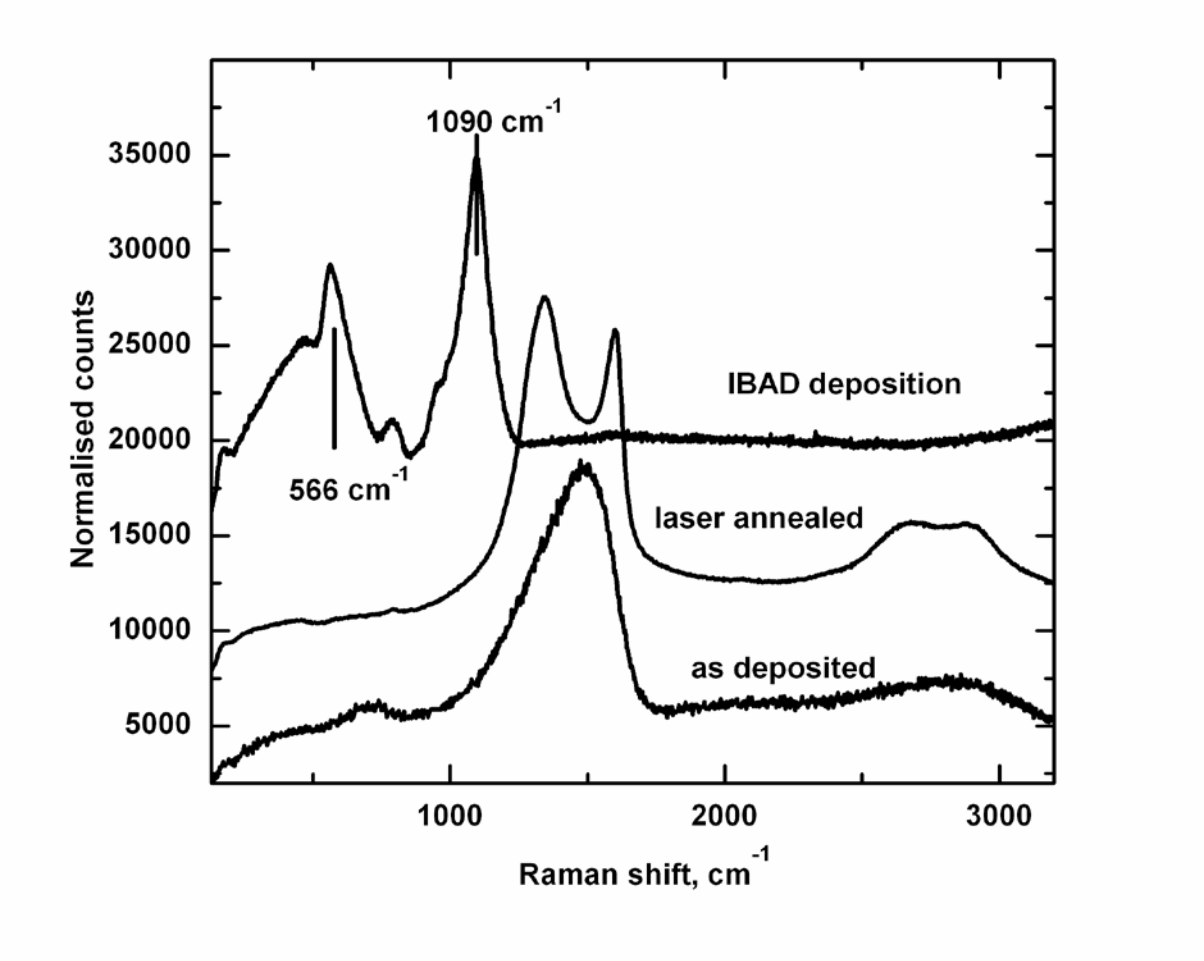
1090 cm-1
566 cm-1
IBAD deposition
laser annealed
as deposited
Normalised counts
Raman shift, cm-1
35000
30000
25000
20000
15000
10000
5000
1000
2000
3000

**Fig. 8.**

## References


[1] R. Riedel, E. Horvath-Bordon, H. J. Kleebe, P. Kroll, G. Miehe, P. A. Van Aken, and S. Lauterbach, Key Engineering Materials **403**, (2009) p. 147

[2] R. Riedel, A. Kienzle, W. Dressler, L. Ruwisch, J. Bill, and F. Aldinger, Nature **382**, (1996) p. 796

[3] J. Vlcek, S. Potocky, J. Cuzek, J. Houska, M. Kormunda, P. Zeman, V. Perina, J. Zemek, Y. Setsuhara, and S. Konuma, J. Vac. Sci. Technol. A **23**(6), (2005) p. 1513

[4] J. Houska, J. Vlcek, S. Hreben, M. M. M. Bilek, and D. R. McKenzie, Europhys. Lett. **76**(3), (2006) p. 512

[5] A. Vijayakumar, R. M. Todi, A. P. Warren, and K. B. Sundaram, Diamond and Related Materials **17**(6), (2008) p. 944

[6] P. A. Ramakrishnan, Y. T. Wang, D. Balzar, L. An, C. Haluschka, R. Riedel, and A. M. Hermann, Applied Physics Letters **76**(20), (2001) p. 3076

[7] N. I. Fainer, M. L. Kosinova, Y. M. Rumyantsev, E. A. Maximovskii, and F. A. Kuznetsov, Journal of Physics and Chemistry of Solids **69**(2-3), (2008) p. 661

[8] R. Wei, Surface and Coatings Technology **203**(5-7), (2008) p. 538

[9] A. M. Hermann, Y. T. Wang, P. A. Ramakrishnan, D. Balzar, L. An, C. Haluschka, and R. Riedel, Journal of the American Ceramic Society **84**(10), (2001) p. 2260

[10] J. Bill, M. Friess, F. Aldinger, and R. Riedel, "Doped silicon carbonitride: Synthesis, characterization and properties," presented at the Materials Research Society Symposium - Proceedings, San Francisco, CA, USA, 1994.

[11] S. R. Shah and R. Raj, Acta Materialia **50**(16), (2002) p. 4093

[12] C. Haluschka, H.-J. Kleebe, R. Franke, and R. Riedel, Journal of the European Ceramic Society **20**(9), (2000) p. 1355

[13] R. Raj, L. An, S. Shah, R. Riedel, C. Fasel, and H. J. Kleebe, Journal of the American Ceramic Society **84**(8), (2001) p. 1803

[14] J. Capek, S. Hreben, P. Zeman, J. Vlcek, R. Cerstvy, and J. Houska, Surface and Coatings Technology **203**, (2008) p. 466

[15] M. Rudolphi, M. Bruns, H. Baumann, and U. Geckle, Diamond and Related Materials **16**(4-7), (2007) p. 1273

[16] J. Houska, J. Vlcek, S. Potocky, and V. Perina, Diamond and Related Materials **16**, (2007) p. 29

[17] K. Banaissa and e. al, IEEE Transactions on Electron Devices **50**(3), (2003) p. 567

[18] J. Houska, M. M. M. Bilek, O. Warschkow, D. R. McKenzie, and J. Vlcek, Physical Review B **72**, (2005) p. 0542041

[19] S. Ma, B. Xu, G. Wu, Y. Wang, F. Ma, D. Ma, K. Xu, and T. Bell, Surface and Coatings Technology **202**(22-23), (2008) p. 5379

[20] D.-H. Kuo and D.-G. Yang, Thin Solid FIlms **374**, (2000) p. 92

[21] H. Hoche, D. Allebrandt, M. Bruns, R. Riedel, and C. Fasel, Surface and Coatings Technology **202**(22-23), (2008) p. 5567

[22] I. V. Afanasyev-Charkin and M. Nastasi, Surface and Coatings Technology **199**(1), (2005) p. 38

[23] N. Fainer, Y. Rumyantsev, M. Kosinova, E. Maximovski, V. Kesler, V. Kirienko, and F. Kuznetsov, Surface and Coatings Technology **201**(22-23), (2007) p. 9269

[24] X. W. Du, Y. Fu, J. Sun, P. Yao, and L. Cui, Materials Chemistry and Physics **103**(2-3), (2007) p. 456

[25] N. Janakiraman and F. Aldinger, Journal of the European Ceramic Society **29**, (2009) p. 163

[26] A. A. Suvorova, T. Nunney, and A. V. Suvorov, Nuclear Instruments and Methods in Physics Research Section B **267**, (2009) p. 1294

[27] C. Gervais, F. Babonneau, L. Ruwisch, R. Hauser, and R. Riedel, Canadian Journal of Chemistry **81**(11), (2003) p. 1359

[28] H. Sachdev, Diamond and Related Materials **12**, (2003) p. 1275
[29] G. Beshkov, S. Lei, V. Lazarova, N. Nedev, and S. S. Georgiev, Vacuum **69**, (2003) p. 301
[30] A. C. Ferrari, S. E. Rodil, and J. Robertson, Diamond and Related Materials **12**(3-7), (2003) p. 905
[31] P. Hoffmann, O. Baake, B. Beckhoff, W. Ensinger, N. Fainer, A. Klein, M. Kosinova, B. Pollakowski, V. Trunova, G. Ulm, and J. Weser, Nuclear Instruments and Methods in Physics Research Section A: Accelerators, Spectrometers, Detectors and Associated Equipment **575**(1-2), (2007) p. 78
[32] R.-G. Duan, J. D. Kuntz, J. E. Garay, and A. K. Mukherjee, Scripta Materialia **50**(10), (2004) p. 1309
[33] C. Haluschka, C. Engel, and R. Riedel, Journal of the European Ceramic Society **20**, (2000) p. 1365
[34] R. Kolb, C. Fasel, V. Liebau-Kunzmann, and R. Riedel, Journal of the European Ceramic Society **26**(16), (2006) p. 3903
[35] R. Weisbarth and M. Jansen, J. Mater. Chem. **13**, (2003) p. 2975
[36] S. Honda, T. Mates, M. Ledinsky, J. Oswald, A. Fejfar, J. Kocka, T. Yamazaki, Y. Uraoka, and T. Fuyuki, Thin Solid FIlms **487**(1-2), (2005) p. 152
[37] N. Mizuochi, M. Ogura, J. Isoya, H. Okushi, and S. Yamasaki, Physica B: Condensed Matter **376-377**, (2006) p. 300
[38] J. Houska, J. Capek, J. Vlcek, M. M. M. Bilek, and D. R. McKenzie, Journal of Vacuum Science and Technology A **25**(5), (2007) p. 1411